What are the building blocks of neuronal computing?

- Sensors to report environmental changes
- Cells that utilize threshold logic and communicate with pulses

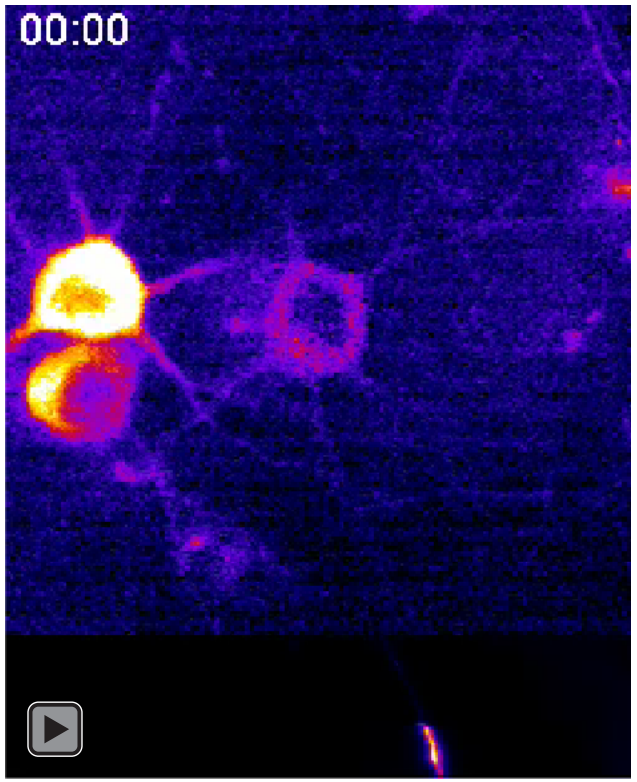

Liu, Li, Marvin& Kleinfeld (under review)

- Connections (synapses) that are unidirectional
- Muscle for movement - the *raison d'etre* for nervous systems

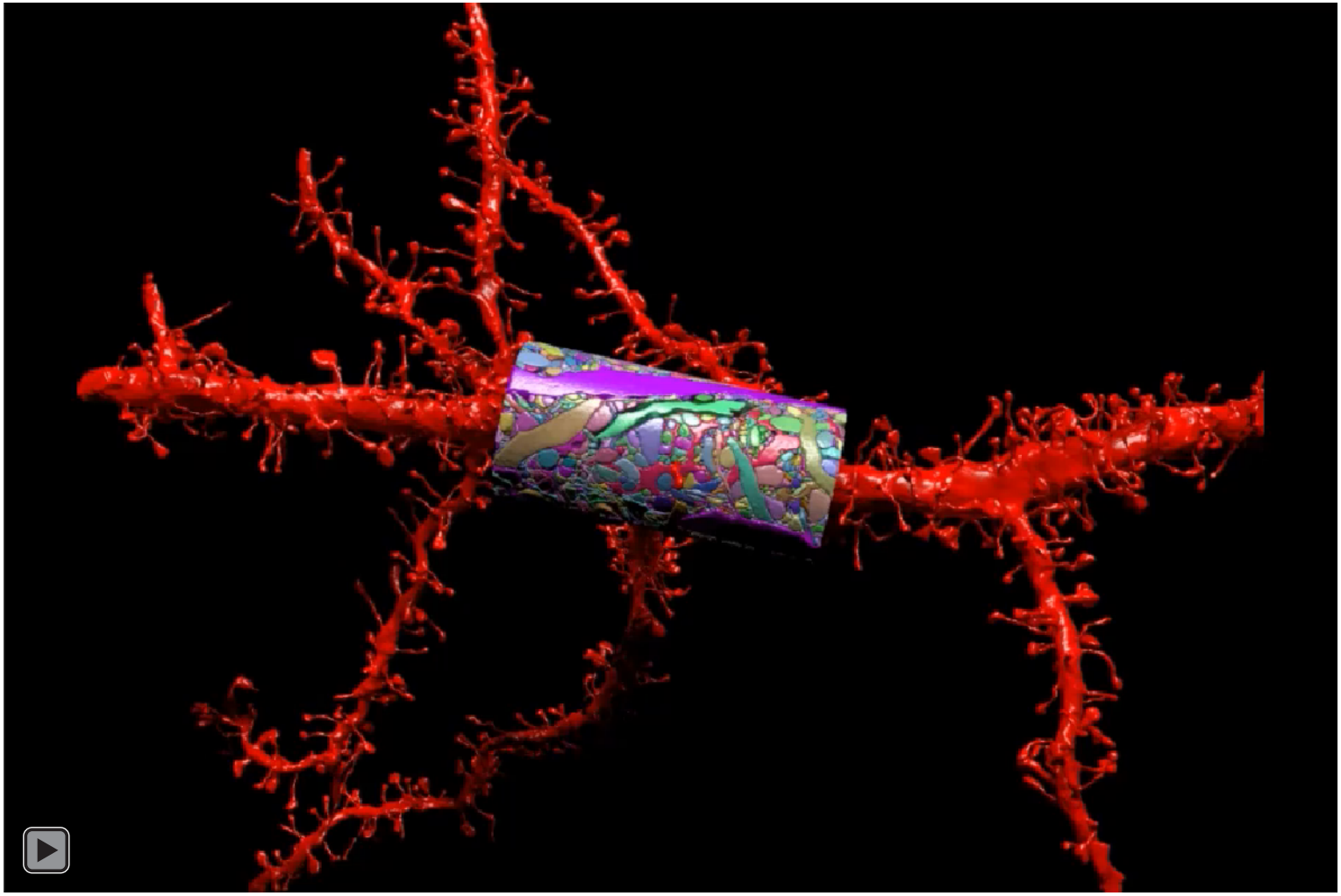

Kasthuri, Hayworth, Berger, Schalek, Conchello, Knowles-Barley, Lee, Vázquez-Reina, Kaynig, Jones, Roberts, Morgan, Tapia, Seung, Roncal, Vogelstein, Burns, Sussman, Priebe, Pfister & Lichtman (Cell 2015)

Mammalian cortical cells come in different shapes; this is *just* a small slice of brain cells

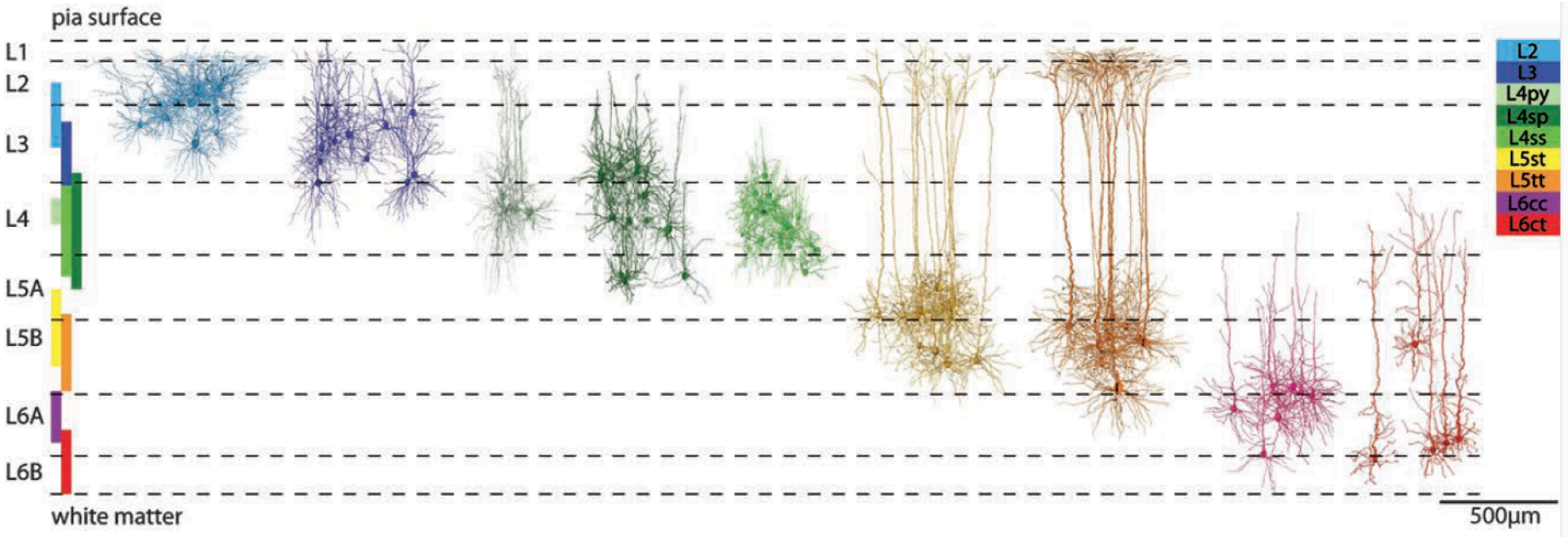

Motta, Berning, Boergens, Staffler, Beining, Loomba, Hennig, Wissler & Helmstaedter (Science 2019)

Neurons reconstructed in the primary input layer, L4, of somatosensory cortex from mouse

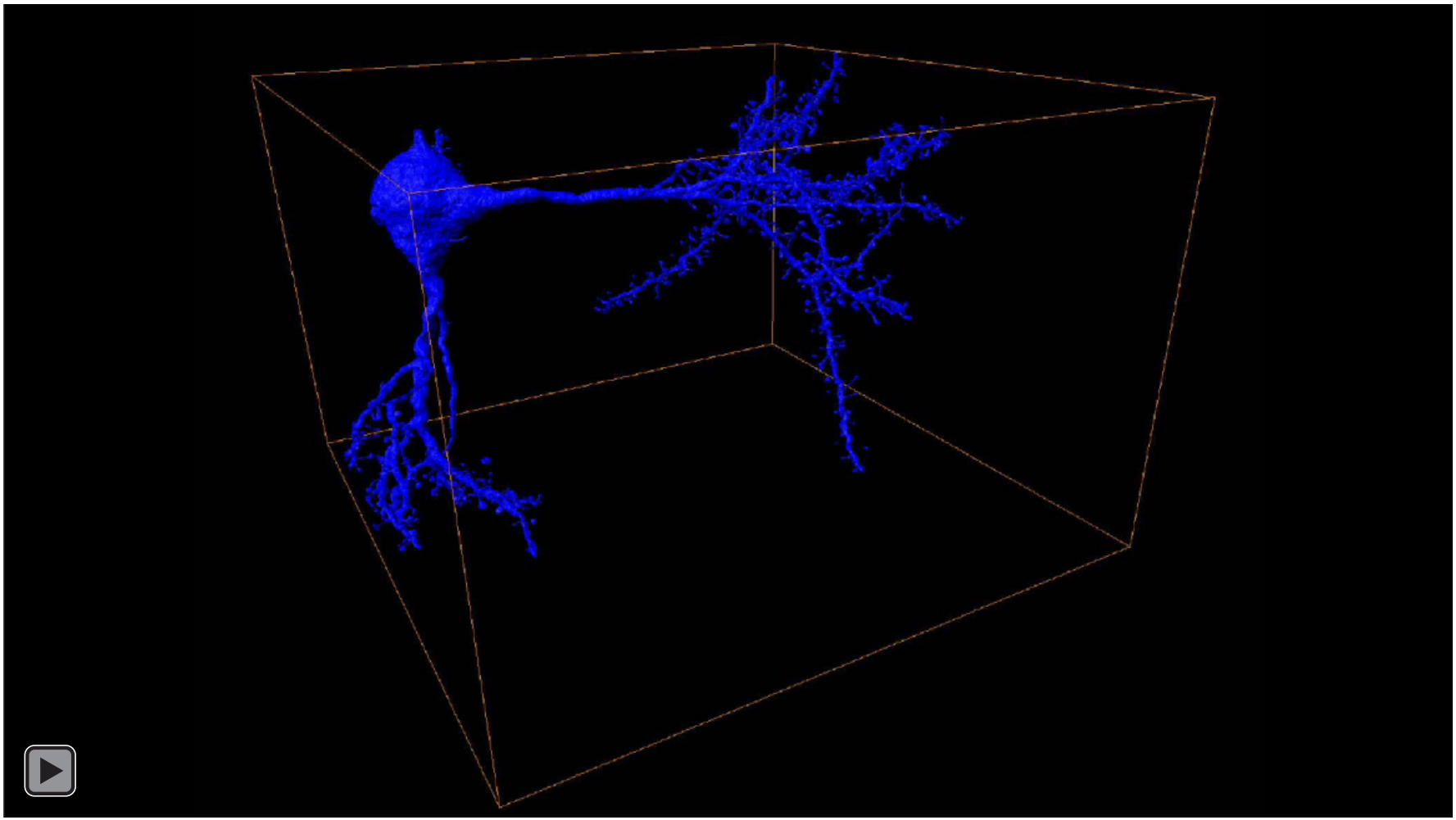

Motta, Berning, Boergens, Staffler, Beining, Loomba, Hennig, Wissler & Helmstaedter (Science 2019)

Basic signaling (data of Deuchers, Thompson & West 2001)

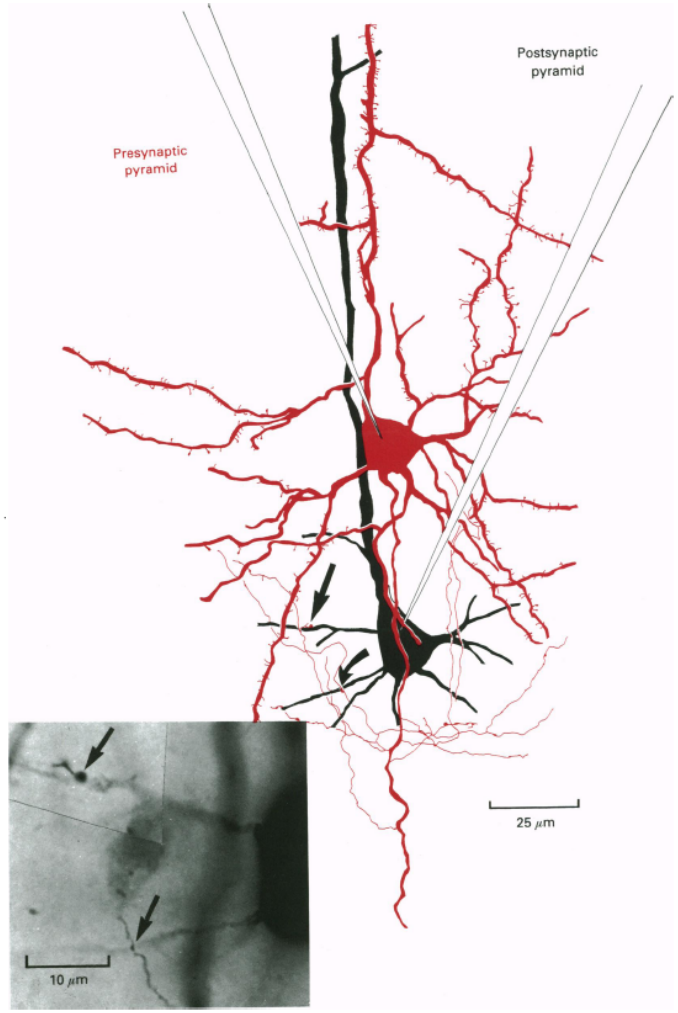

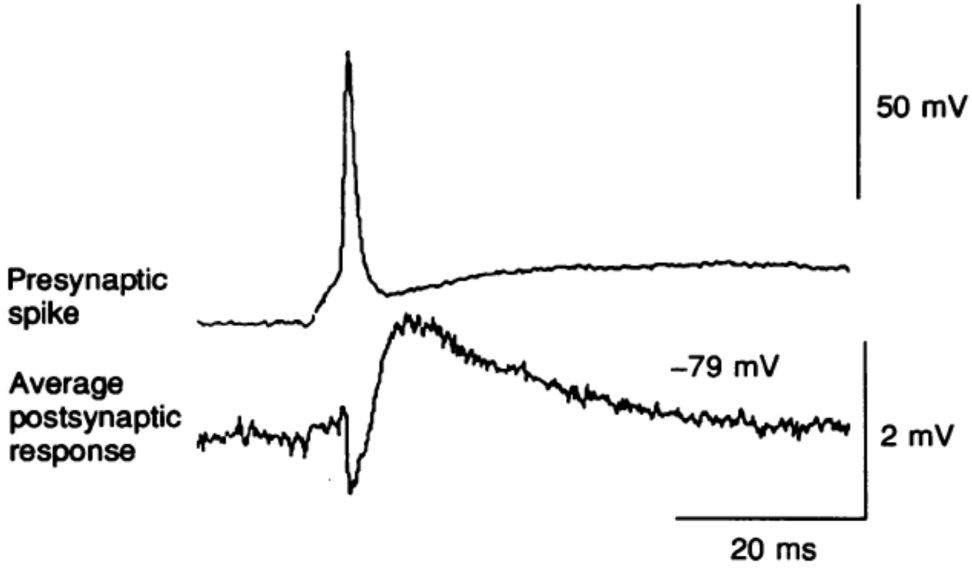

Signaling involves release of vesicles that contain transmitter molecules and are 30 to 50 nm in diameter

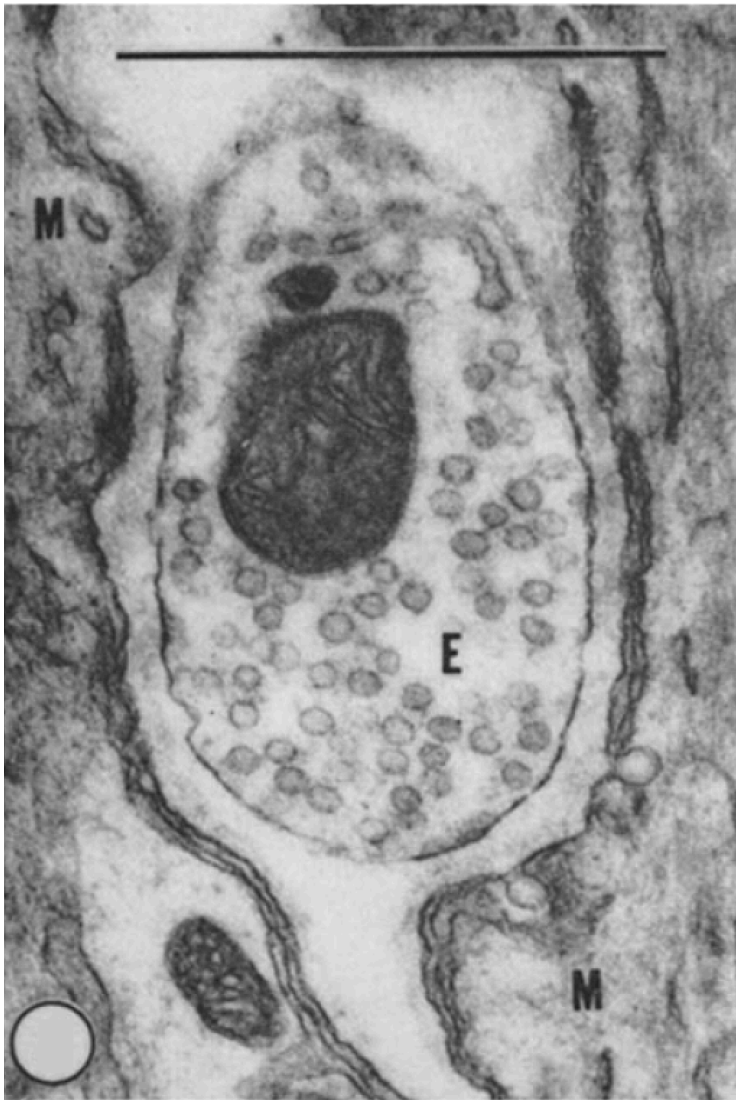

Neuron partition ions to build two or more voltage levels

Resting Potential: Electrochemical Equilibrium

$$V = \frac{K_B T}{e} \ln \frac{[X]_{out}}{[X]_{in}}$$

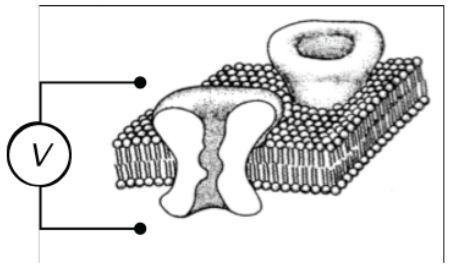

$V = -65\,mV$

Out of Equilibrium

- For $V > V_x$ current flows into cell: $I_x > 0$
- For $V < V_x$ current flows out of cell: $I_x < 0$
- *I-V* curve (current-voltage):

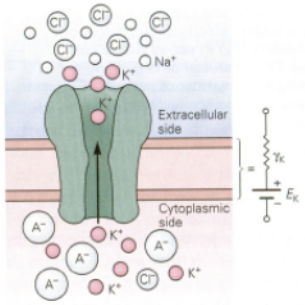

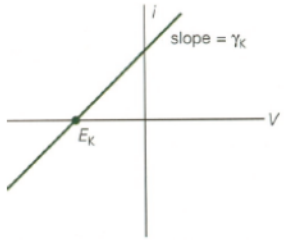

$$I_K = \gamma_K (V - V_K)$$

Multiple Kinds of Ions

- Several *I-V* curves in parallel:

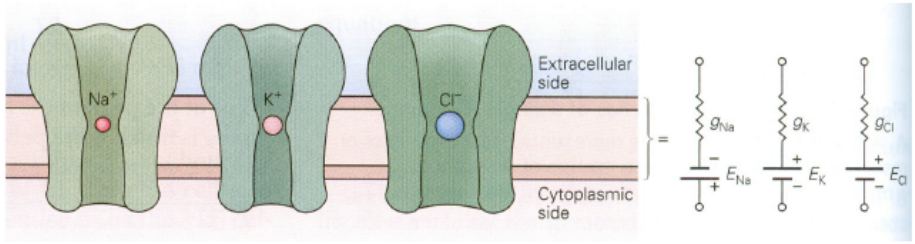

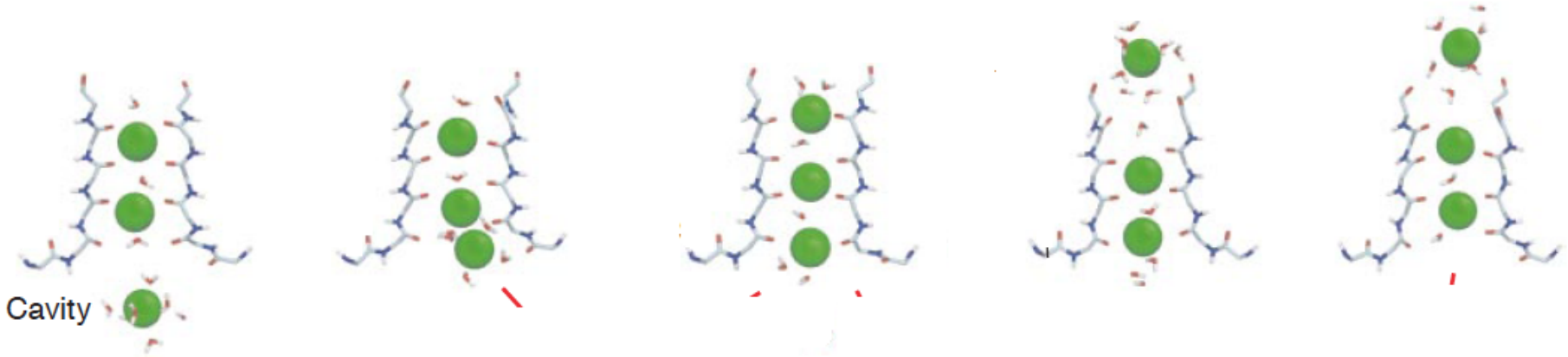

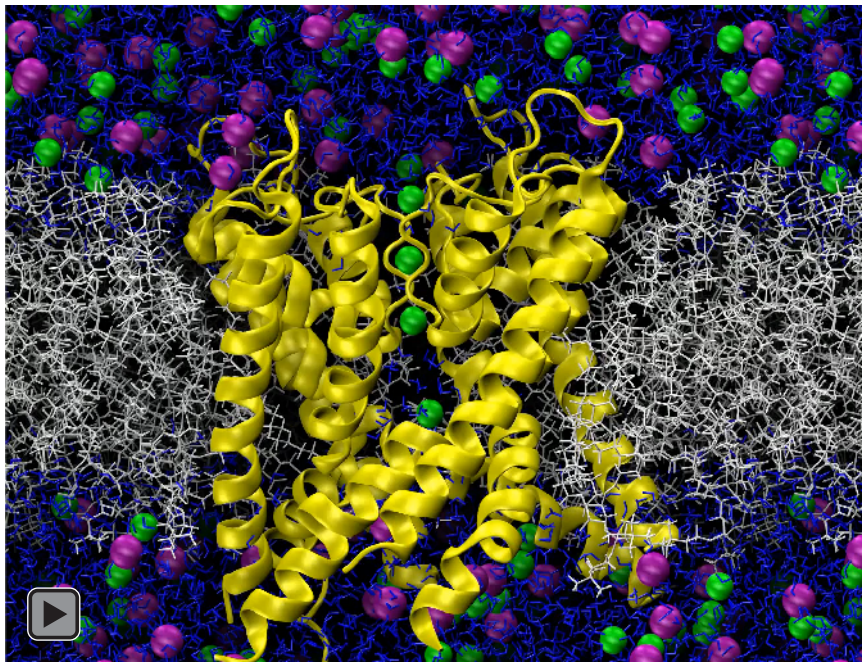

Berneche & Roux (Nature 2001)

Threshold instability leads to a pulse

Real Data from Lobster Axon

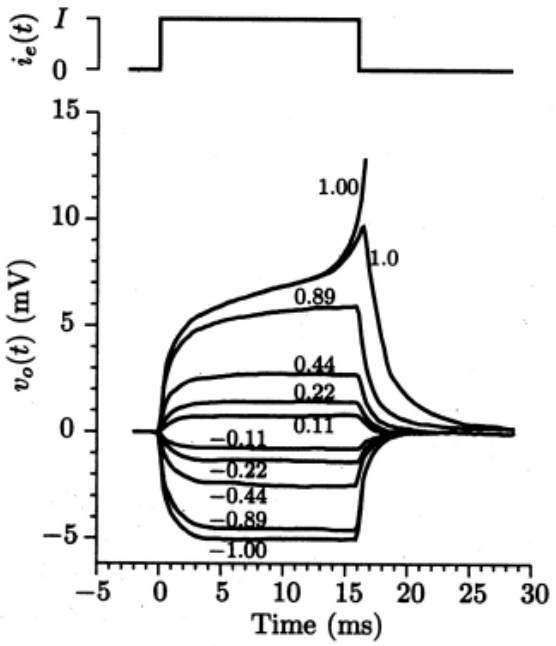

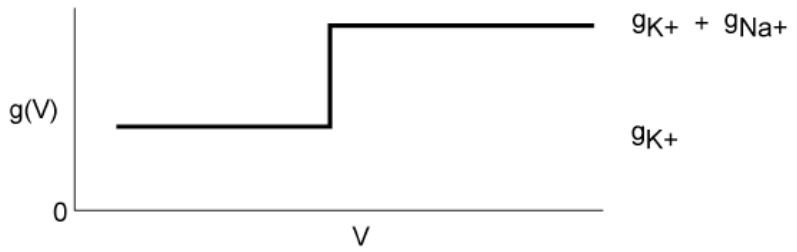

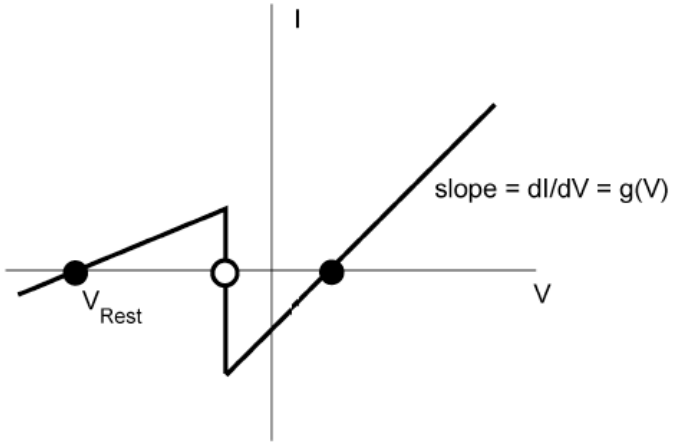

I-V curves for Squid Axon from Action Potential Trigger to Recovery

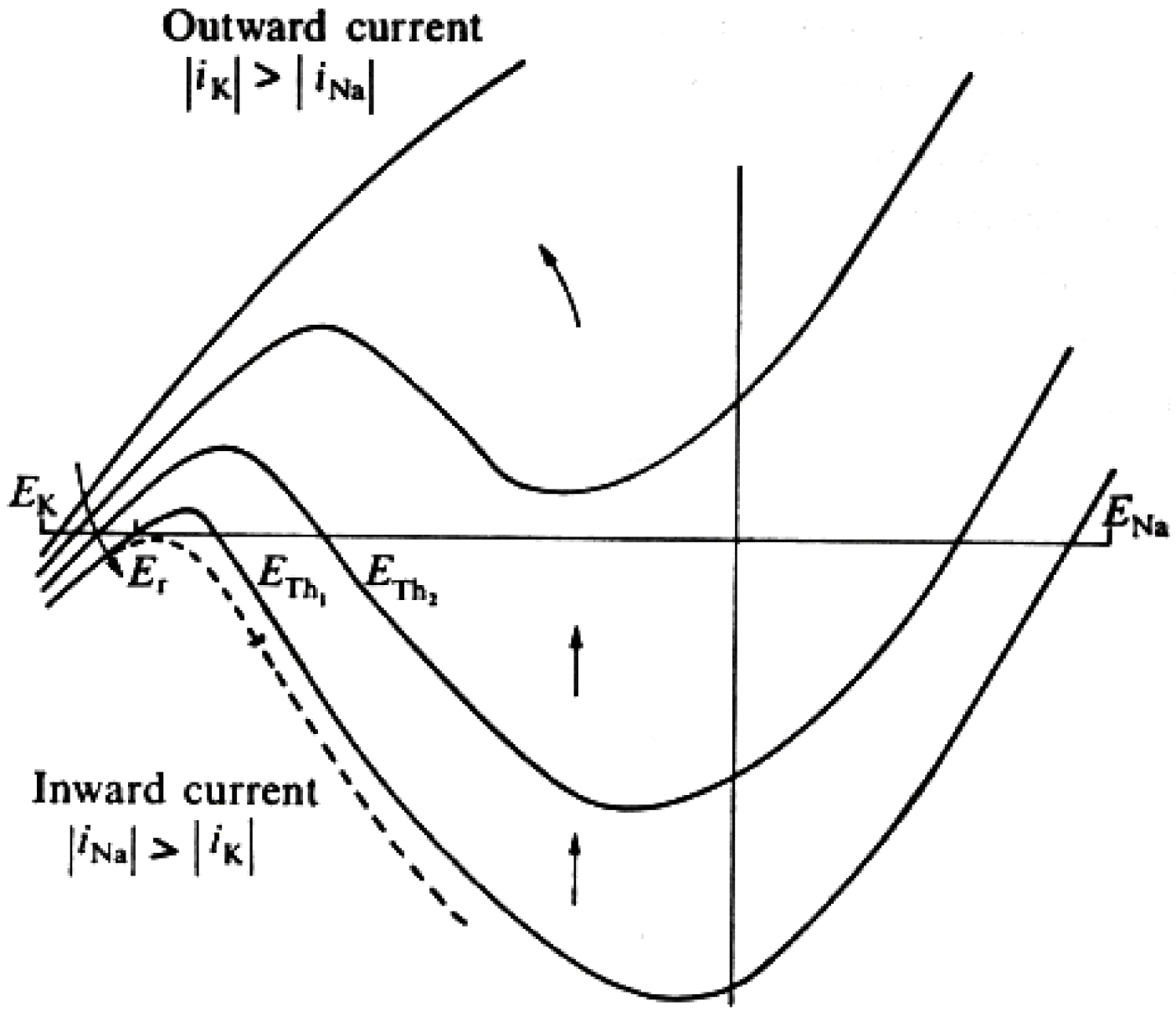

chapt_1_ap_iv_vs_time.eps

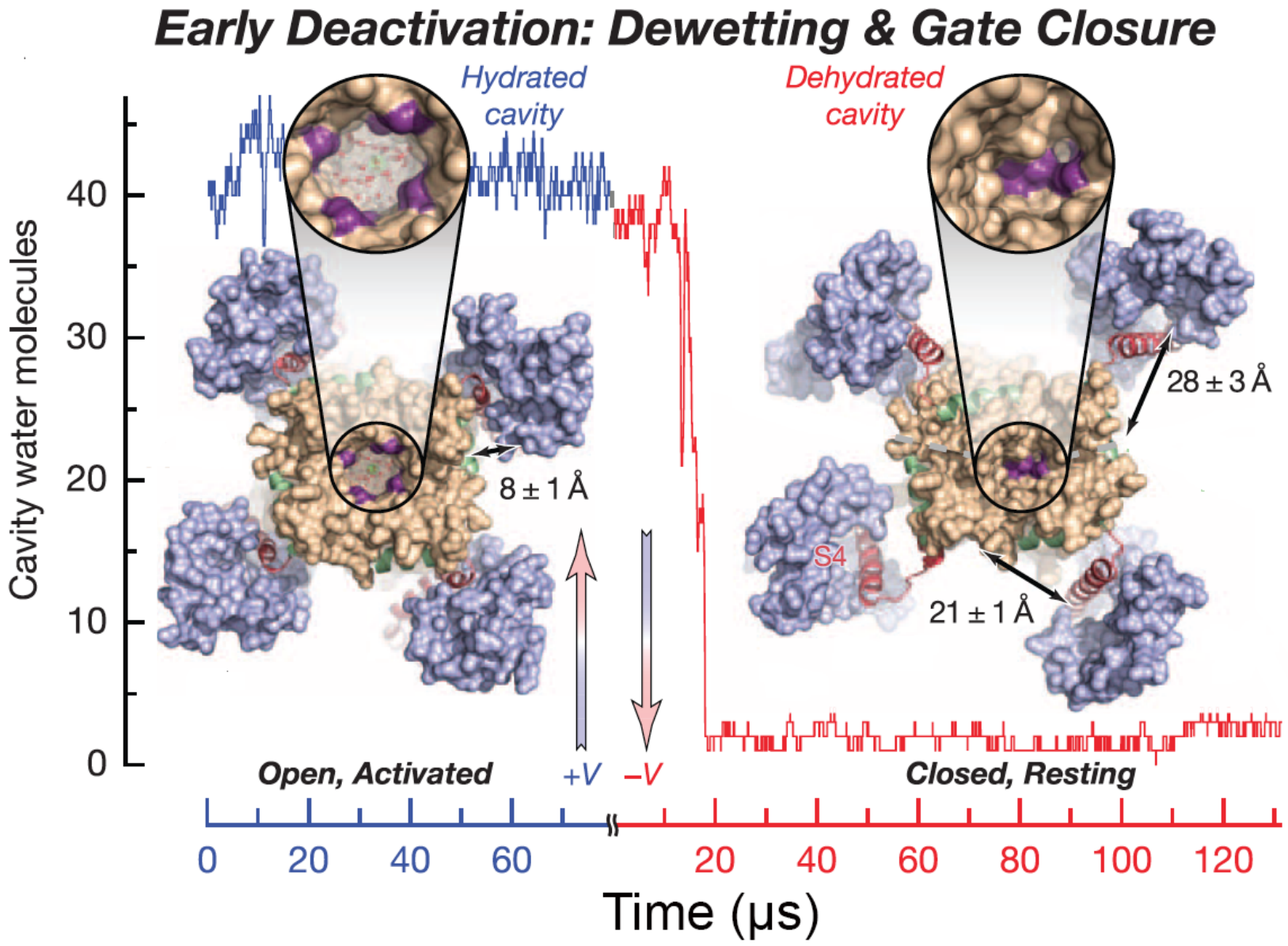

Jensen, Jogini, Borhani, Leffler, Dror & Shaw (Nature 2012)
following data of: Long, Campbell & MacKinnon (Science 2005); Long, Tao, Campbell & MacKinnon (Nature 2007)

Fig. 3. Mechanistic model for voltage gating. Subjecting the activated state (**1**) to hyperpolarizing voltage initiates S4 inward movement and VSD–pore loosening. Ion depletion of the pore cavity (**2**)—coupled to inward motion of a single S4—leads to pore hydrophobic collapse. Closure of upper (Ile^{402} in $K_v1.2$) and lower gates [PVP motif; Leu^{331} (S5)–Pro^{405} (S6) side-chain interchange (*21*)] halts conduction (**3**). S4 continues inward; as S4 completes its inward motion, the S4-S5 linker helix moves fully down and the VSDs loosen from the pore, consolidating the resting state (**4**). Subjecting the resting state to depolarizing voltage drives S4 outward. When all four S4 and S4-S5 linker helices are fully up (**5**) and all VSDs repack against the pore, the lower gate becomes destabilized; the **4** → **5** transition constitutes the rate-limiting step in the activation process. Lower gate fluctuation triggers pore opening and partial pore rehydration (water molecules cooperatively enter the cavity) that allow ion entry and initial outward conduction (**6**); the **5** → **6** transition is essentially voltage-independent. The presence of ions drives complete pore rehydration that pushes fully open the upper and lower gates, returning the channel to the activated state (**1**). The lateral position of the VSDs (circles) relative to the pore domain (squares) is shown schematically (extracellular view).

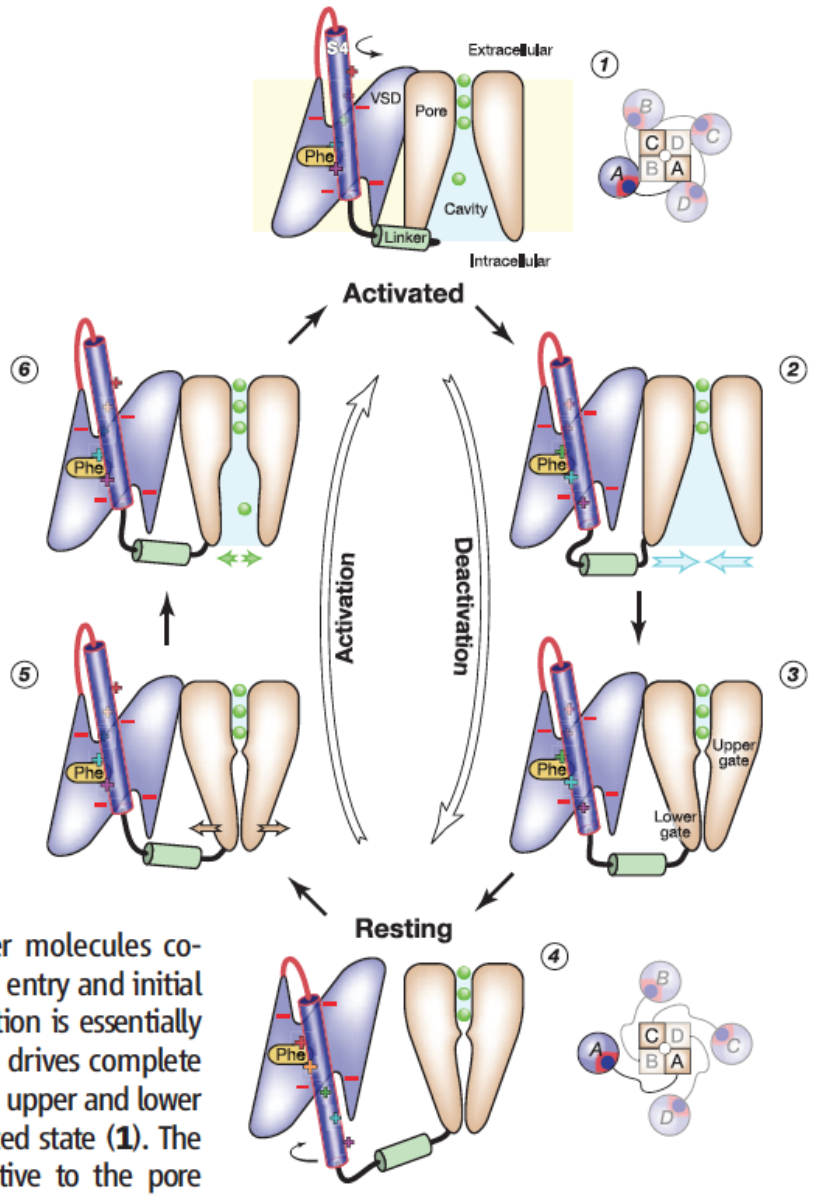

Jensen, Jogini, Borhani, Leffler, Dror & Shaw (Nature 2012)

Voltage levels and threshold yield mixed analog and digital computing on the scale of order k_BT/e

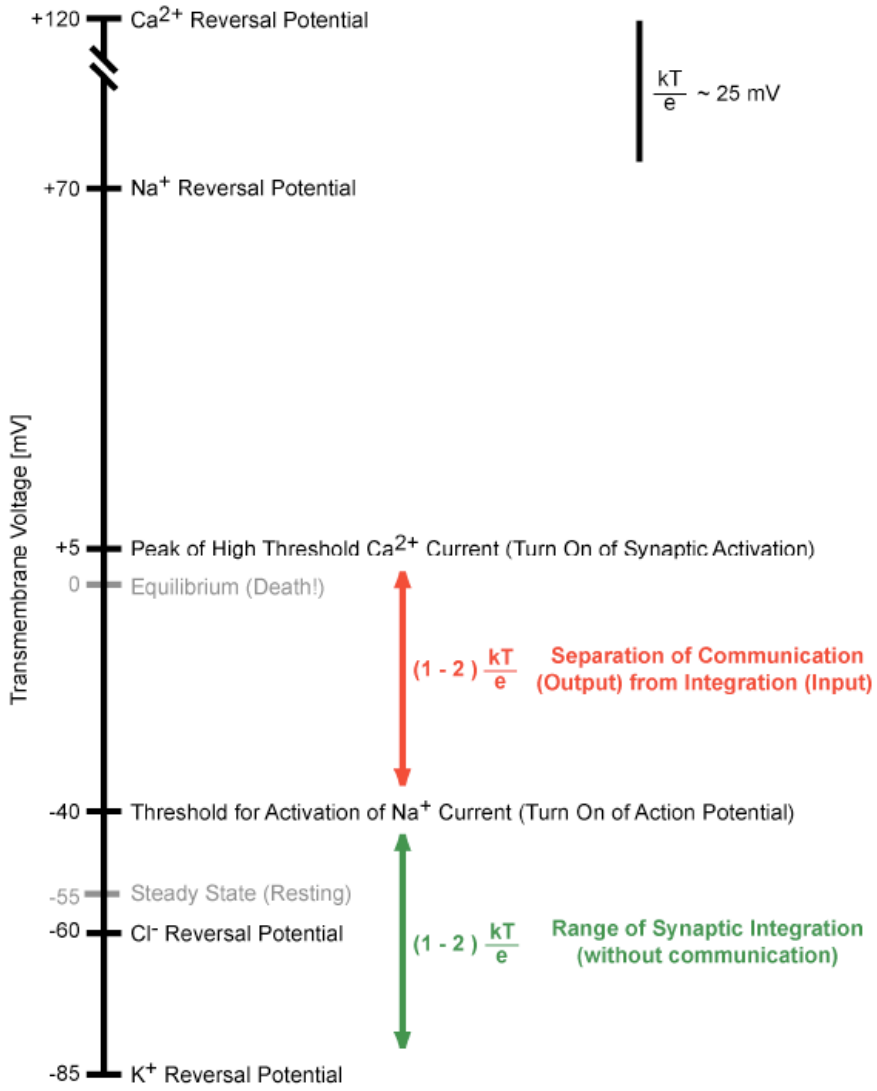

N-type Ca^{2+} currents in presynaptic terminals initiate synaptic vessel fusion and set maximum voltage level

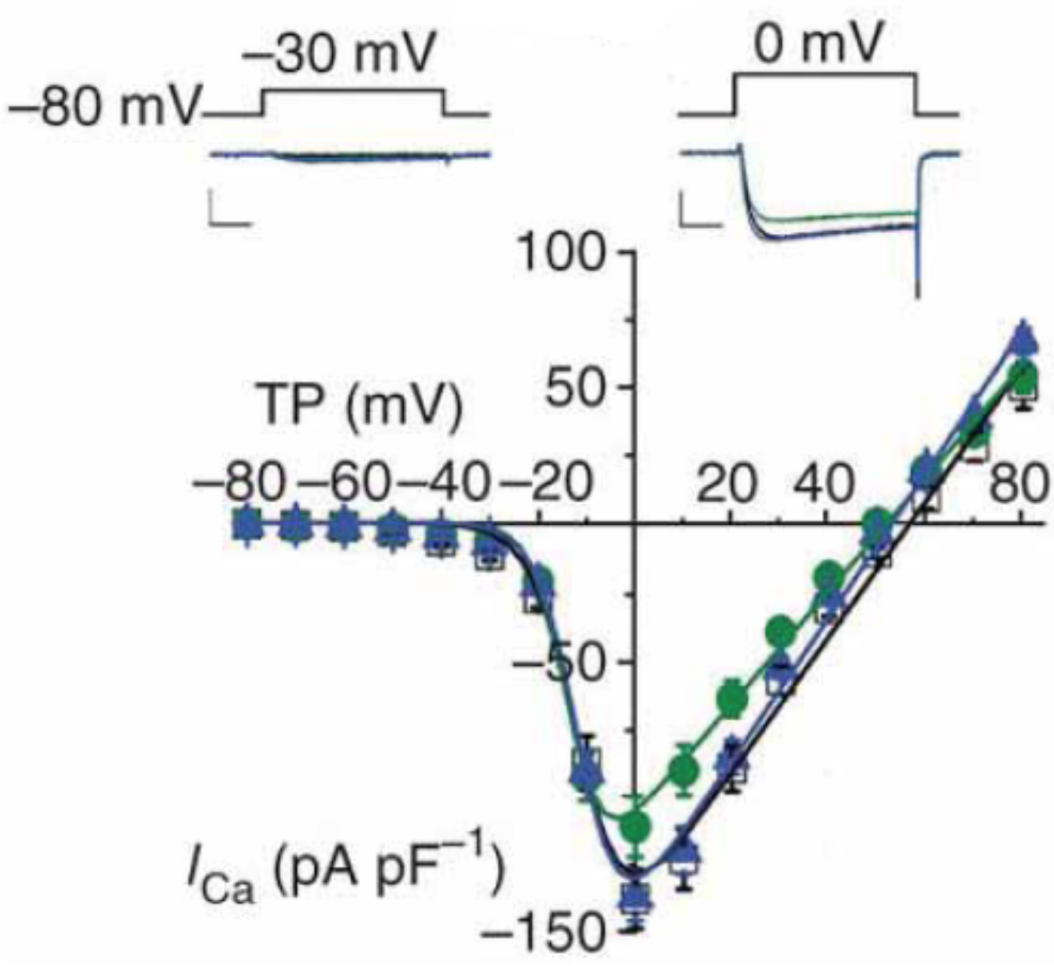

Neurons use an elaborate physiochemical scheme for unidirectional (synaptic) communication

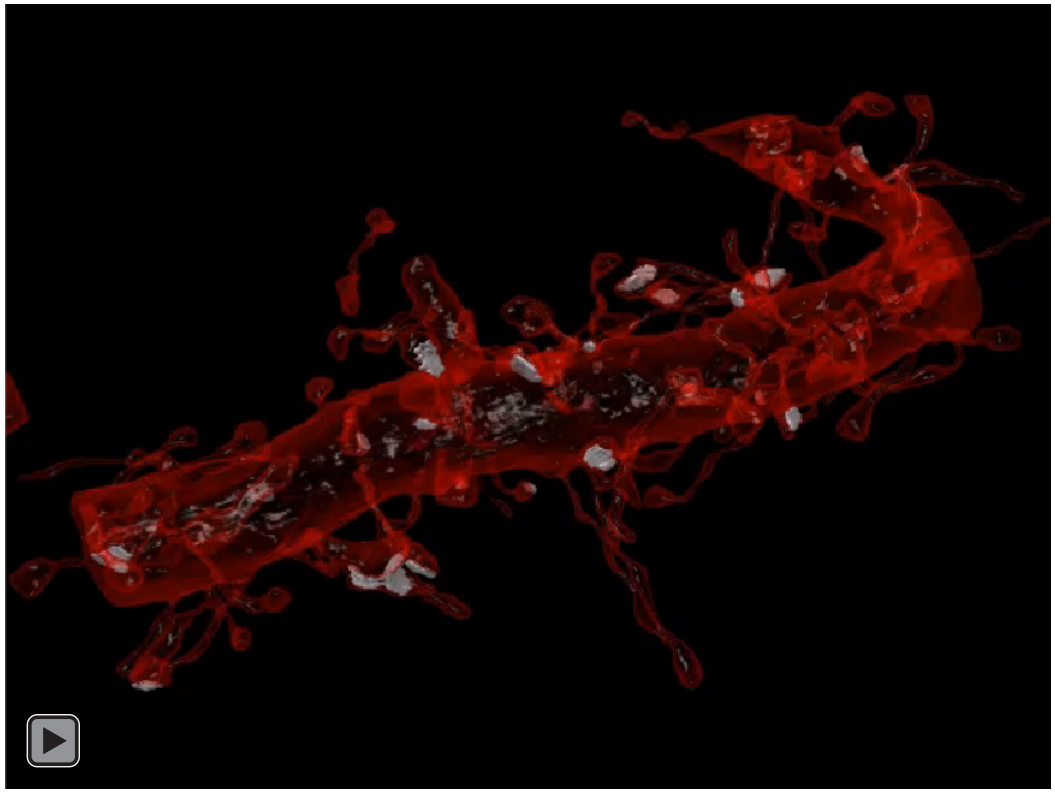

Kasthuri, Hayworth, Berger, Schalek, Conchello, Knowles-Barley, Lee, Vázquez-Reina, Kaynig, Jones, Roberts, Morgan, Tapia, Seung, Roncal, Vogelstein, Burns, Sussman, Priebe, Pfister & Lichtman (Cell 2015)

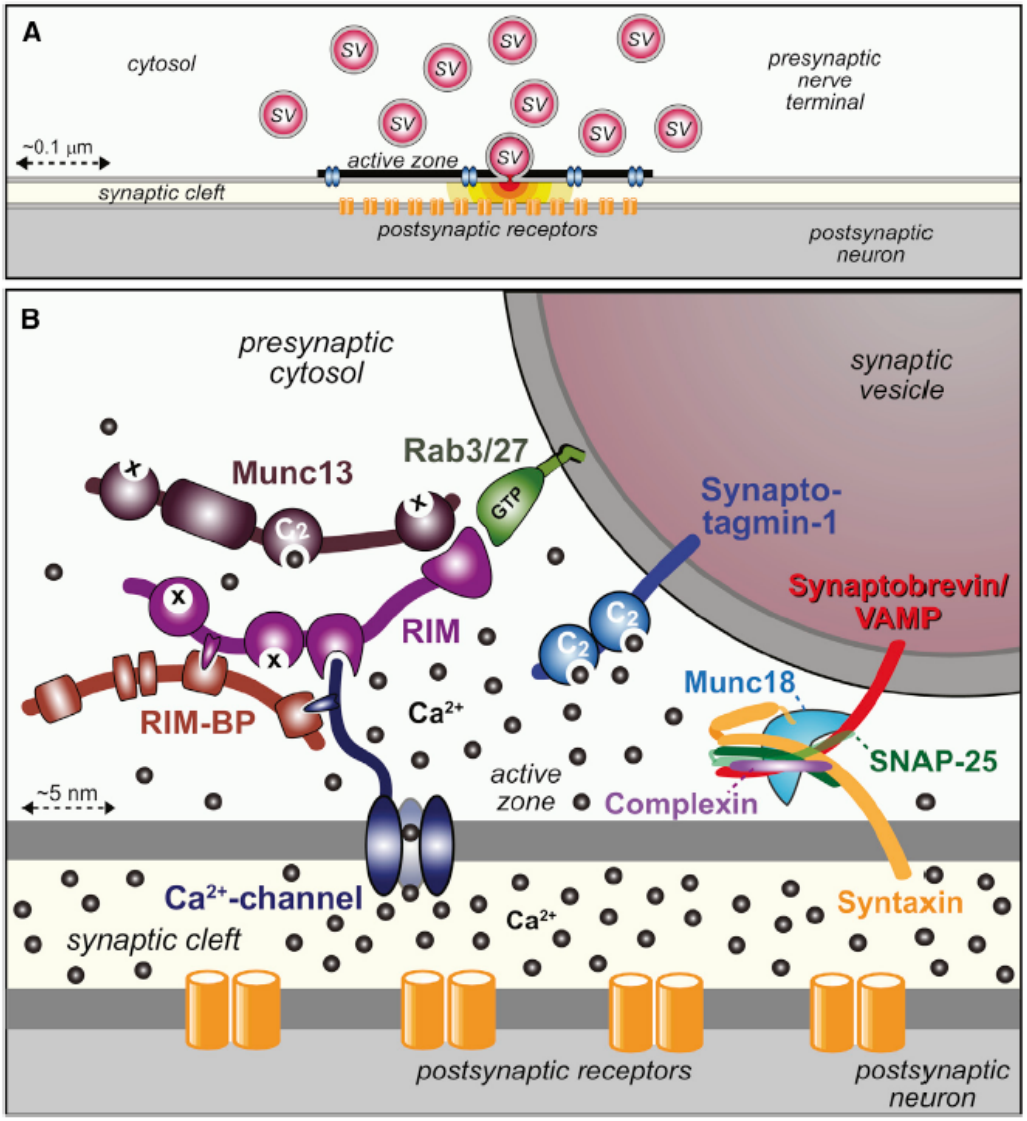

Figure 1. Organization of the Presynaptic Release Machinery

(A) Drawing of a synapse with synaptic vesicles (SV, red), an active zone containing Ca^{2+} channels (blue), and a postsynaptic cluster of receptors (orange). One vesicle in the active zone is depicted in the process of fusing, with red neurotransmitters emitting from the fusion pore.

(B) Schematic of the molecular machinery mediating Ca^{2+}-triggered vesicle fusion. The drawing depicts a segment of a docked synaptic vesicle on the top right and the presynaptic active zone in the middle. The three functional elements of the neurotransmitter release machinery are depicted from right to left. On the right, the core fusion machine composed of the SNARE/SM protein complex is shown; this machine comprises the SNARE proteins synaptobrevin/VAMP, syntaxin-1, and SNAP-25 and the SM protein Munc18-1. The Ca^{2+} sensor synaptotagmin-1 is depicted in the middle; it is composed of a short intravesicular sequence, a single transmembrane region, and two cytoplasmic C2 domains that bind Ca^{2+}, and it functions using complexin (bound to the SNARE complex) as an assistant. The active zone protein complex containing RIM, Munc13, and RIM-BP and a Ca^{2+} channel in the presynaptic plasma membrane is shown on the left. In this protein complex, RIM binding to specific target proteins coordinates all three functions of the active zone: RIM binding to vesicular rab proteins (Rab3 and Rab27 isoforms) mediates vesicle docking; RIM binding to the central priming factor Munc13 activates vesicle priming; and RIM binding to the Ca^{2+} channel, both directly and indirectly via RIM-BP, recruits the Ca^{2+} channels within 100 nm of the docked vesicles for fast excitation-secretion coupling. The overall design of the neurotransmitter release machinery depicted here enables in a single nanodevice fast and efficient triggering of release in response to an action potential by combining a fusion machine with a Ca^{2+} trigger and an active zone protein complex that positions all elements into appropriate proximity

Sudhof (Neuron 2013)

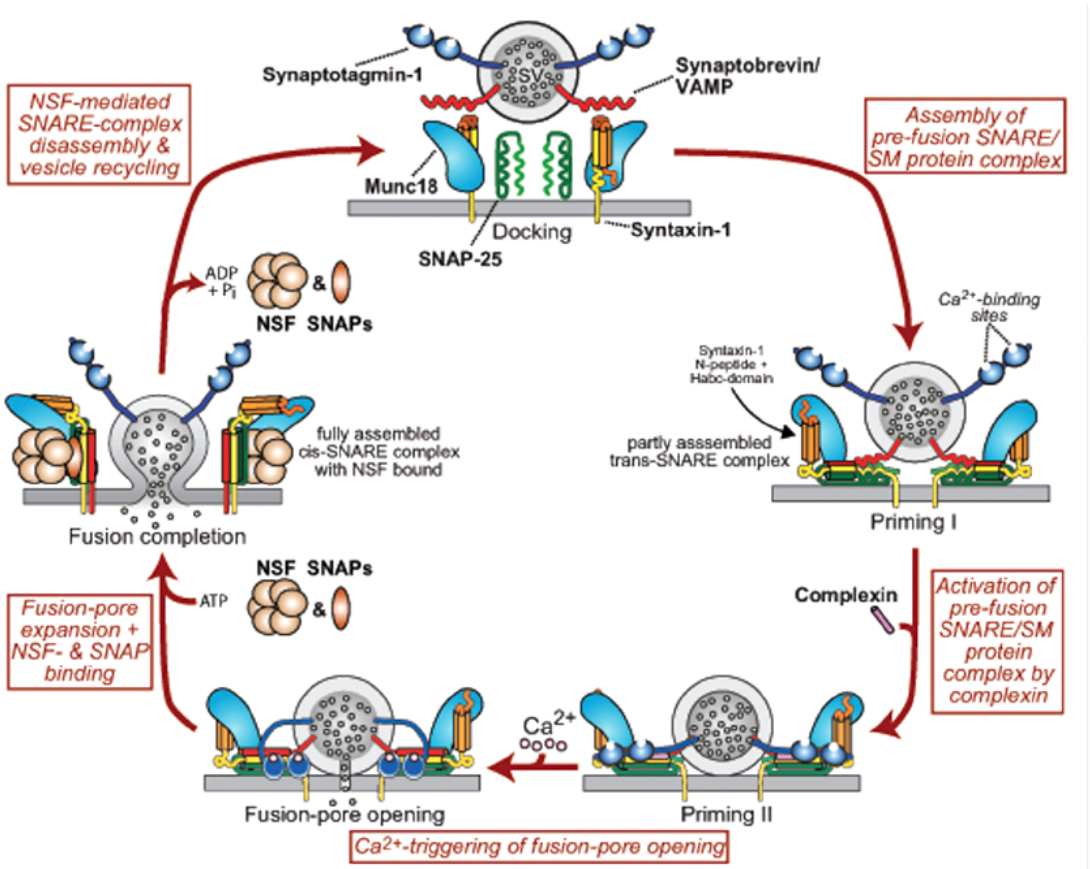

Figure 2. Schematic of the SNARE/SM Protein Cycle Mediating Fusion and the Role of Synaptotagmin and Complexin in Ca^{2+} Triggering of Fusion

SNARE and SM proteins undergo a cycle of assembly and disassembly, such that the vesicular SNARE protein synaptobrevin assembles during priming into a *trans*-SNARE complex with the plasma membrane SNARE proteins syntaxin-1 and SNAP-25. Prior to SNARE complex assembly, syntaxin-1 is present in a closed conformation in which its Habc domain folds back onto its SNARE motif; this conformation precludes SNARE complex assembly, and syntaxin-1 has to "open" for SNARE complex assembly to initiate. Moreover, prior to SNARE complex assembly, Munc18-1 is associated with monomeric syntaxin-1 when syntaxin-1 is in a closed conformation; as syntaxin-1 opens during SNARE complex assembly, Munc18-1 alters the mode of its binding to syntaxin-1 by binding to assembling *trans*-SNARE complexes via interacting with the syntaxin-1 N-peptide. Once SNARE complexes are partially assembled, complexin binds to further increase their priming. The "superprimed" SNARE/SM protein complexes are then substrate for Ca^{2+}-triggered fusion pore opening by Ca^{2+} binding to synaptotagmin, which causes an interaction of synaptotagmin with SNAREs and phospholipids. However, even before Ca^{2+} triggering, synaptotagmin likely at least partly interacts with the fusion machinery as evidenced by the unclamping of spontaneous mini release in Syt1 knockout neurons. After fusion pore opening, the resulting *cis*-SNARE complexes are disassembled by the NSF/SNAP ATPases, and vesicles are recycled, refilled with neurotransmitters, and reused for release

Sudhof (Neuron 2013)

Why is this all not so simple to understand?

- Connections are dense, non-randomly distributed and nonrandomly weighted
- Few strong connections in a sea of weak connections

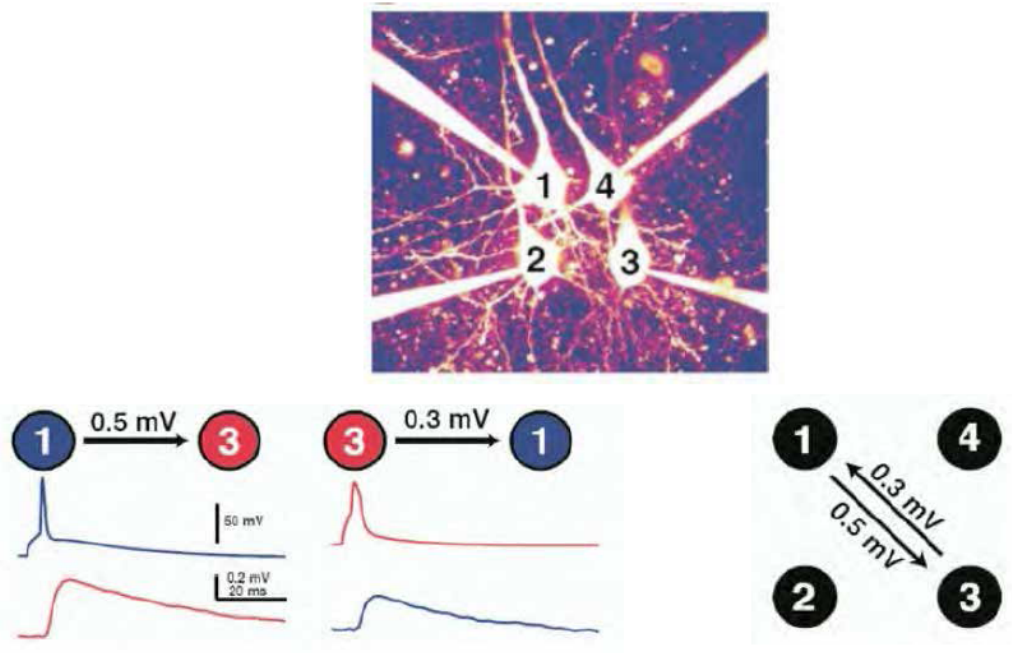

- Information about the presence and strength of connections
- But false negatives due to slicing artefacts

Song, Sjöström, Reigl, Nelson & Chklovskii (PLoS Biology)

Overrepresentation of bidirectional motifs

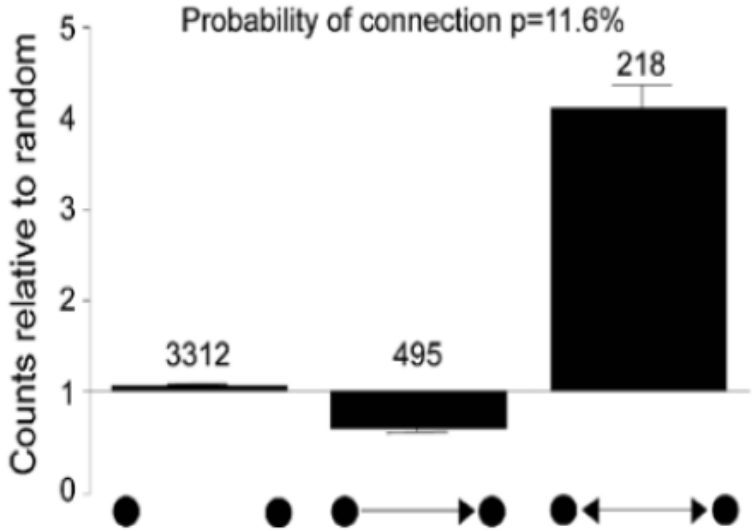

L5 pyramidal cells, Song et al. (2005)

Connection strengths are variable and their distribution has a long tail

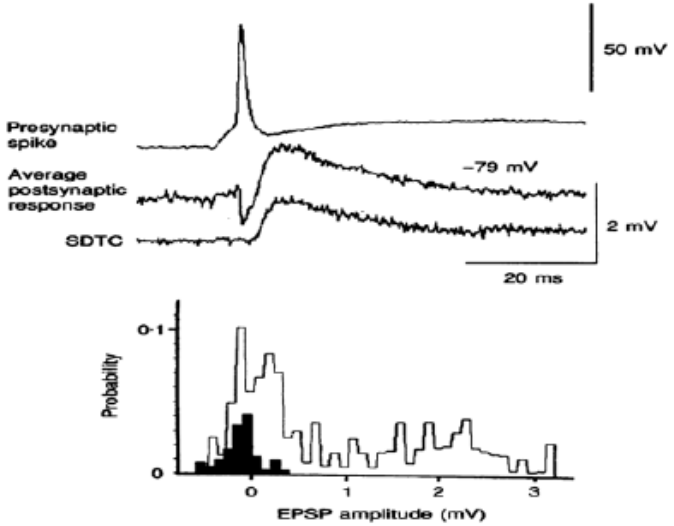

L5/6 pyramidal cells, Deuchars, West, Thomson (1994)

Mapping receptive fields with two-photon calcium imaging and reverse correlation

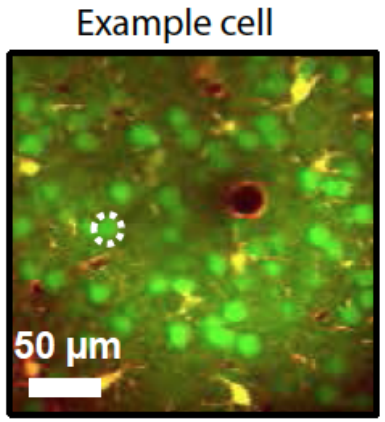

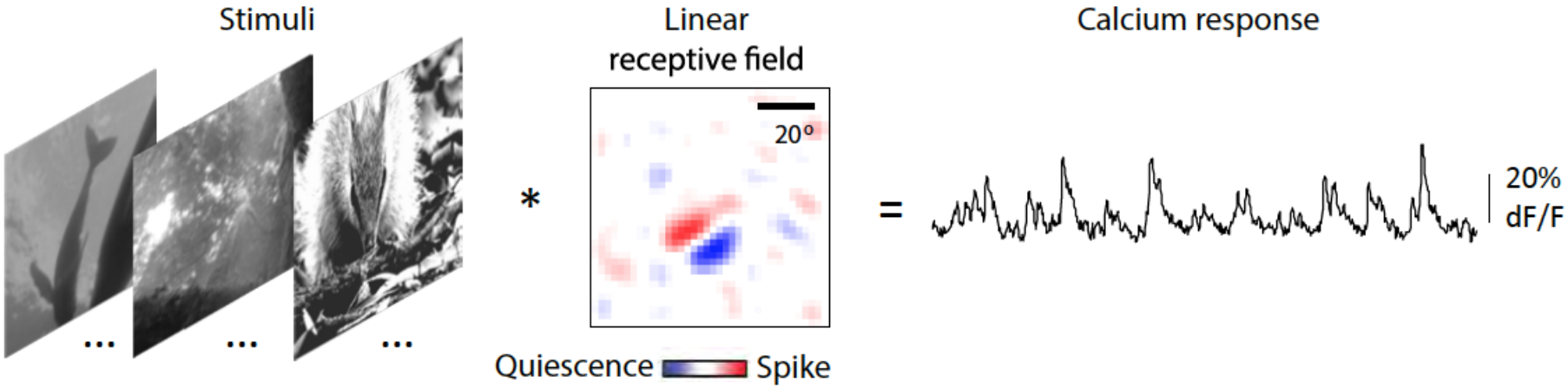

Cossell, Iacaruso, Muir, Houlton, Sader, Ko, Hofer & Mrsic-Flogel (Nature 2015)

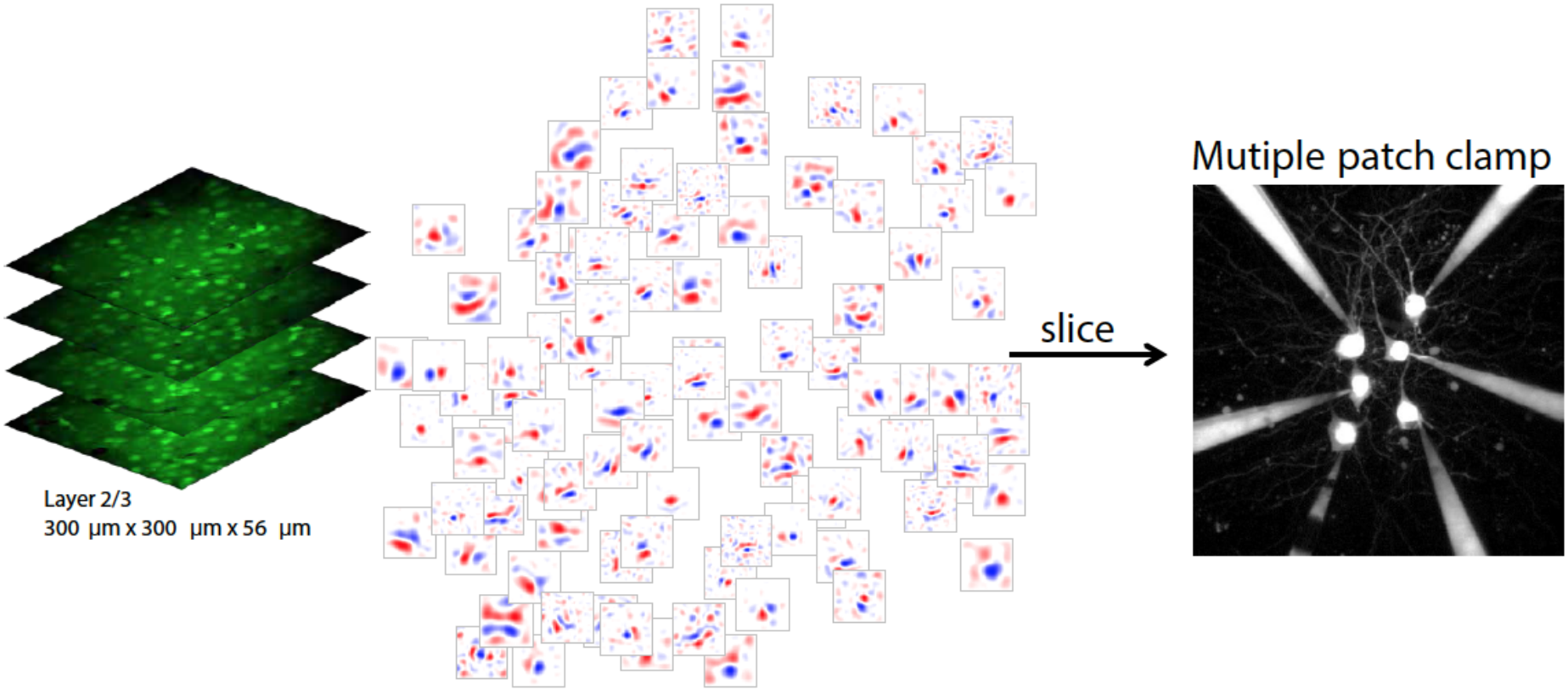

Cossell, Iacaruso, Muir, Houlton, Sader, Ko, Hofer & Mrsic-Flogel (Nature 2015)

Relating synaptic connections to receptive fields

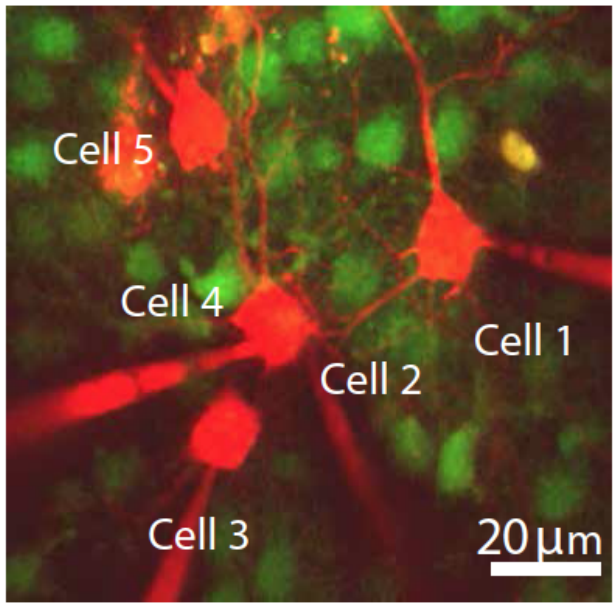

Exp : 20130522, Motif 2

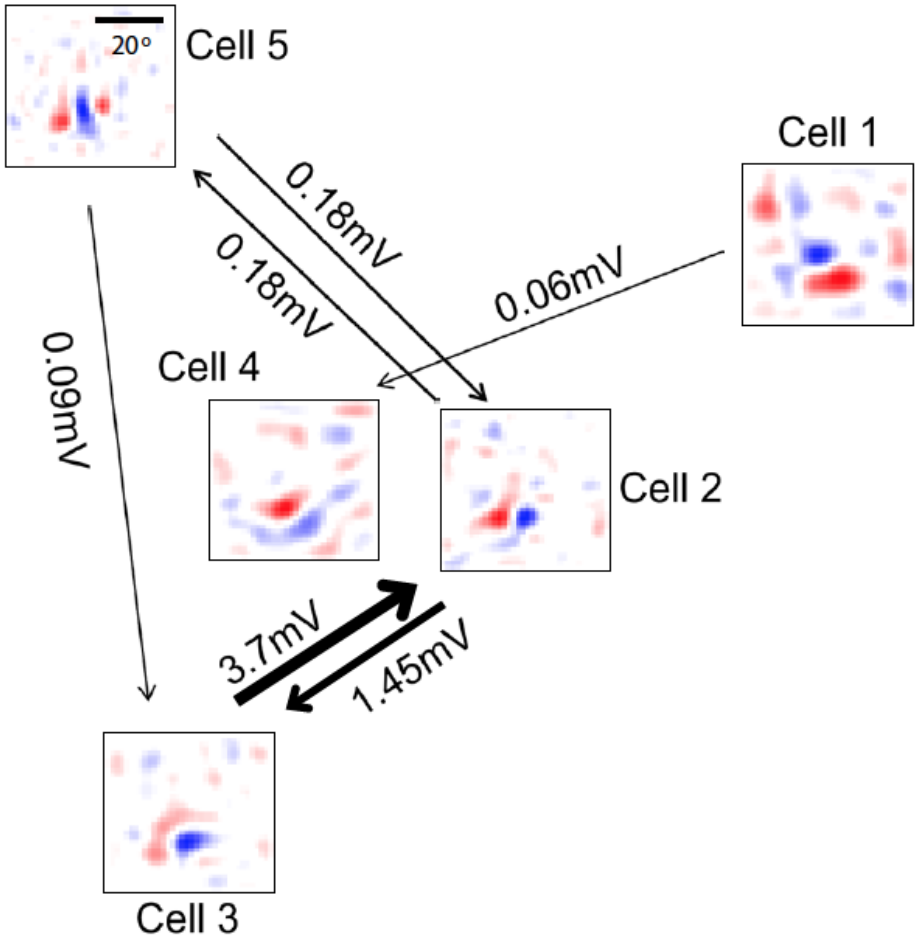

Cossell, Iacaruso, Muir, Houlton, Sader, Ko, Hofer & Mrsic-Flogel (Nature 2015)

Similarity of receptive fields predicts probability, strength, and reciprocity of synaptic connections

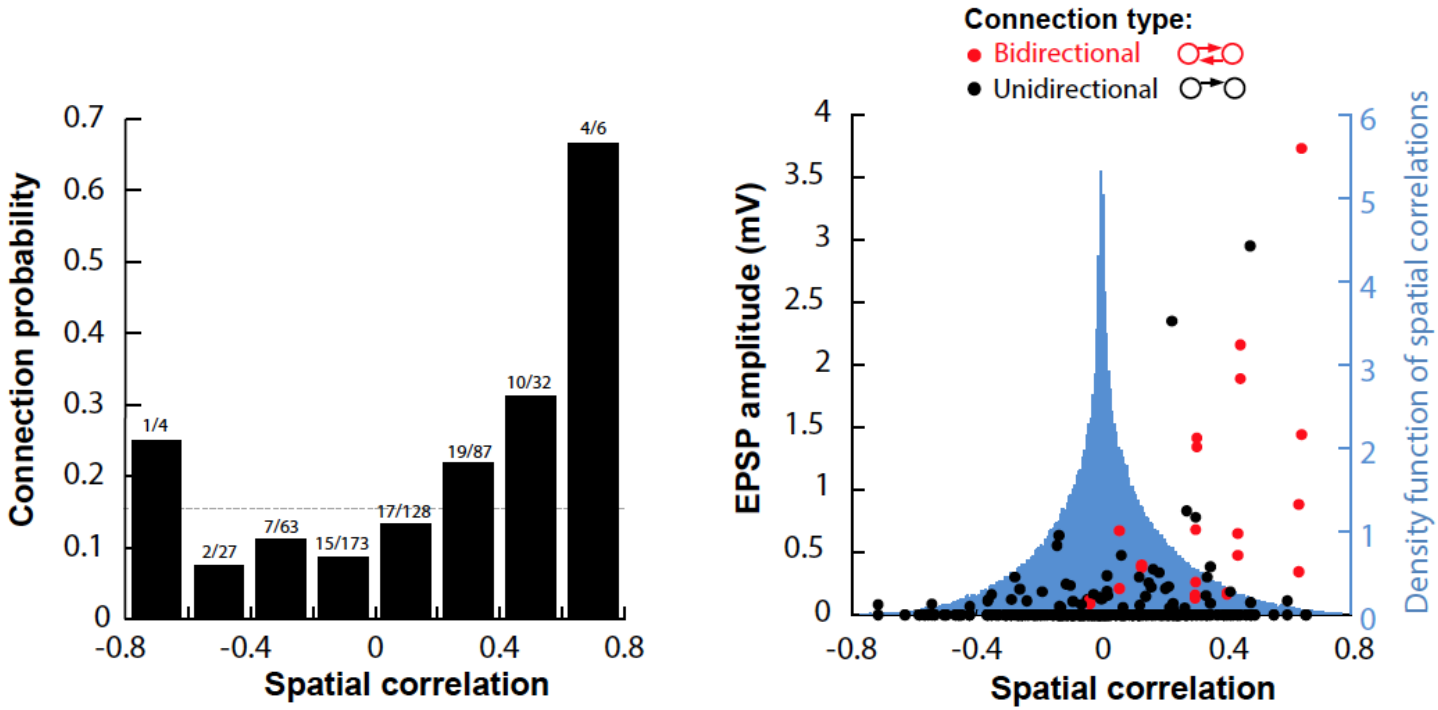

Spatial correlation is a strong predictor of connectivity

Cell pairs with positive correlations are more likely to connect with strong connections

Reciprocal connections are stronger and exist between cell pairs with similar receptive fields

Cossell, Iacaruso, Muir, Houlton, Sader, Ko, Hofer & Mrsic-Flogel (Nature 2015)

At least in primary visual cortex, the evidence implies that
neurons are connected by a few strong synapses in a sea of weak synapses

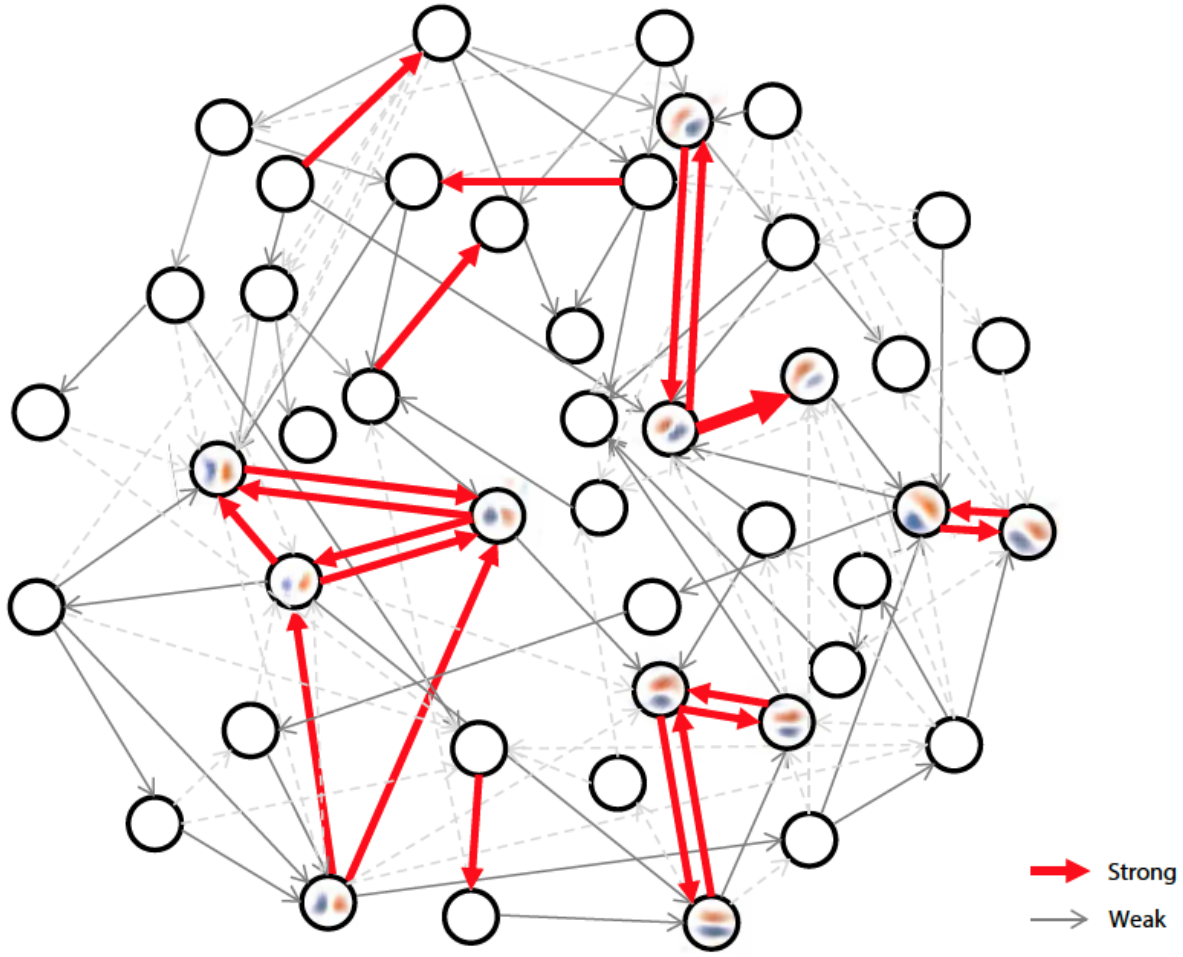

What about the noise from all the "weak" connections*?

A (very) rough worst-case estimate, using

$$\Delta V_{\text{strong-synapse}} \; / \; \Delta V_{\text{weak-synapse}} \;\sim\; 2 \text{ mV} / 100 \;\mu\text{V} \;\sim\; 20$$

and $\sqrt{N} \;\sim\; \sqrt{10{,}000} \;\sim\; 100$

leads to

Synchronous sensory input: $M \, \Delta V_{\text{strong-synapse}} \gg \sqrt{N} \, \Delta V_{\text{weak-synapse}}$

$\therefore \; M \gg 5$

Asynchronous sensory input: $\sqrt{M} \, \Delta V_{\text{strong-synapse}} \gg \sqrt{N} \, \Delta V_{\text{weak-synapse}}$

$\therefore \; M \gg 25$

Conclude that preferred pathways of 10 - 100 connections, or 0.01 to 0.1 of total ($M \ll N$), can in principle dominate the computational role of a circuit.

Can we explain neuronal responses in a "simple" way?

RESOURCE
https://doi.org/10.1038/s41593-019-0550-9
nature neuroscience

A large-scale standardized physiological survey reveals functional organization of the mouse visual cortex

Saskia E. J. de Vries[1,5*], Jerome A. Lecoq[1,5*], Michael A. Buice[1,5*], Peter A. Groblewski[1], Gabriel K. Ocker[1], Michael Oliver[1], David Feng[1], Nicholas Cain[1], Peter Ledochowitsch[1], Daniel Millman[1], Kate Roll[1], Marina Garrett[1], Tom Keenan[1], Leonard Kuan[1], Stefan Mihalas[1], Shawn Olsen[1], Carol Thompson[1], Wayne Wakeman[1], Jack Waters[1], Derric Williams[1], Chris Barber[1], Nathan Berbesque[1], Brandon Blanchard[1], Nicholas Bowles[1], Shiella D. Caldejon[1], Linzy Casal[1], Andrew Cho[1], Sissy Cross[1], Chinh Dang[1], Tim Dolbeare[1], Melise Edwards[1], John Galbraith[1], Nathalie Gaudreault[1], Terri L. Gilbert[1], Fiona Griffin[1], Perry Hargrave[1], Robert Howard[1], Lawrence Huang[1], Sean Jewell[2], Nika Keller[1], Ulf Knoblich[1], Josh D. Larkin[1], Rachael Larsen[1], Chris Lau[1], Eric Lee[1], Felix Lee[1], Arielle Leon[1], Lu Li[1], Fuhui Long[1], Jennifer Luviano[1], Kyla Mace[1], Thuyanh Nguyen[1], Jed Perkins[1], Miranda Robertson[1], Sam Seid[1], Eric Shea-Brown[1,3], Jianghong Shi[3], Nathan Sjoquist[1], Cliff Slaughterbeck[1], David Sullivan[1], Ryan Valenza[1], Casey White[1], Ali Williford[1], Daniela M. Witten[2,4], Jun Zhuang[1], Hongkui Zeng[1], Colin Farrell[1], Lydia Ng[1], Amy Bernard[1], John W. Phillips[1], R. Clay Reid[1] and Christof Koch[1]

To understand how the brain processes sensory information to guide behavior, we must know how stimulus representations are transformed throughout the visual cortex. Here we report an open, large-scale physiological survey of activity in the awake mouse visual cortex: the Allen Brain Observatory Visual Coding dataset. This publicly available dataset includes the cortical activity of nearly 60,000 neurons from six visual areas, four layers, and 12 transgenic mouse lines in a total of 243 adult mice, in response to a systematic set of visual stimuli. We classify neurons on the basis of joint reliabilities to multiple stimuli and validate this functional classification with models of visual responses. While most classes are characterized by responses to specific subsets of the stimuli, the largest class is not reliably responsive to any of the stimuli and becomes progressively larger in higher visual areas. These classes reveal a functional organization wherein putative dorsal areas show specialization for visual motion signals.

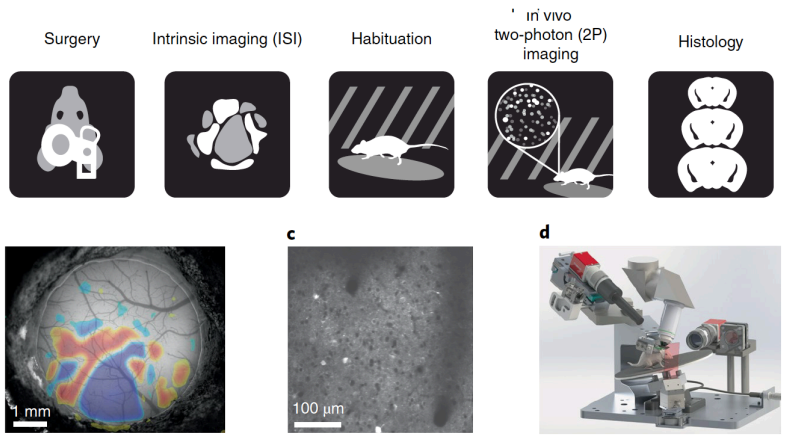

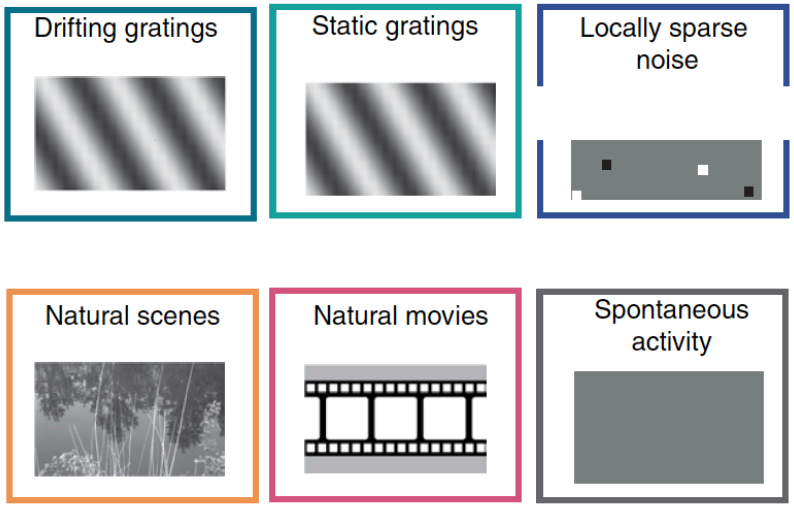

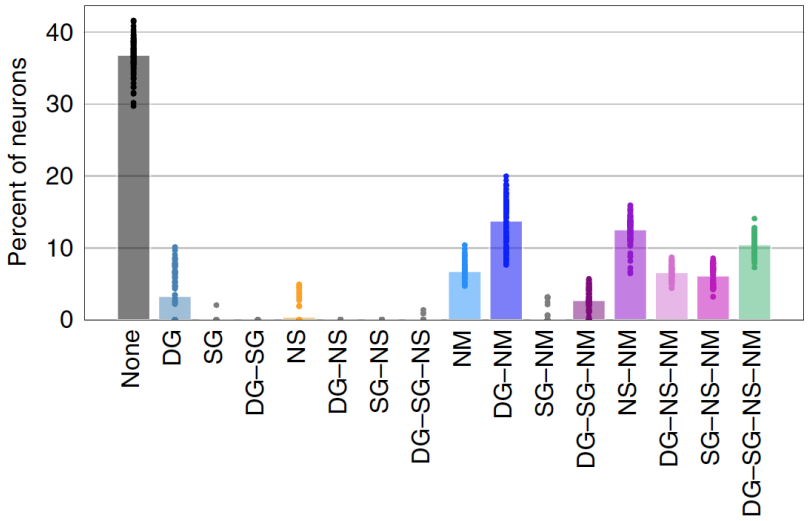

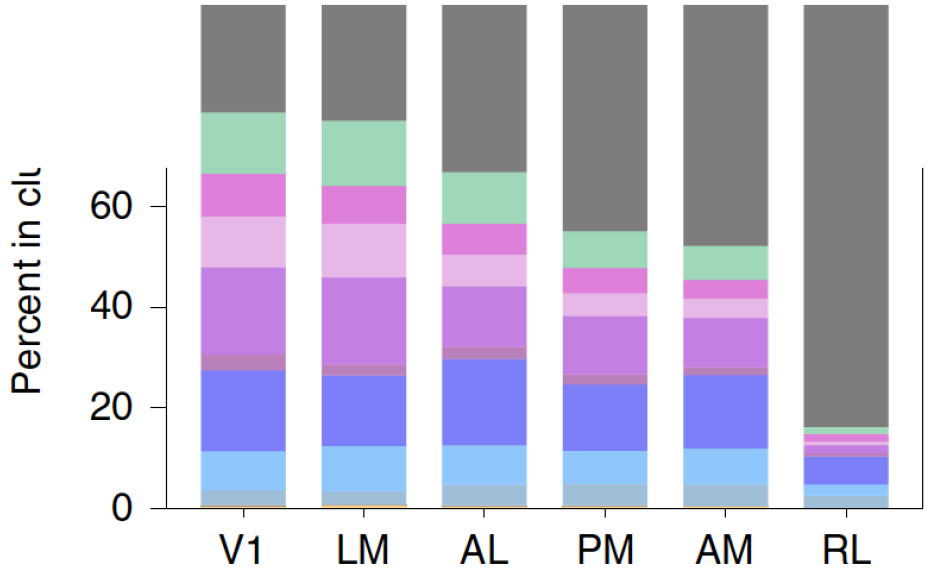

Answer = Sometimes, when recording close to the periphery